From Chip to Converter: A Complete Cost Model for Power Electronics Converters

Gabriel Domingues-Olavarría, Pontus Fyhr, Avo Reinap, Mats Andersson, and Mats Alaküla

***Abstract*—The unified knowledge on power converter design and manufacturing technology establishes a powerful tool, where the cost and topology realization can be analyzed simultaneously. This paper collects the design practice and cost estimation of various components in a power electronics converter and unites that to a choice of the assembling and manufacturing processes and resulting cost of the complete converter. The outcome of this work specifies the power converter at predefined power level and cooling condition and demonstrates the cost drivers of the complete unit depending on production volumes. As a case study, the cost of an inverter for a full electric or hybrid vehicle application is estimated and the results are compared with figures available in the literature, yielding the conclusion that the validity of such figures is highly dependent on production volumes and power levels. The essence of this paper is a set of general, reliable, and fast design models and production charts, in accordance with realistic cost estimates for the sake of system optimization and development of cost effective electric drives from small series to large volumes.**

***Index Terms*—Converters, costs, design methodology, manufacturing economics, power electronics.**

I. Introduction

DUE to an increase in environmental awareness [1] and concerns regarding dependence on fossil fuels [2], the interest in power electronics converters (PEC) has increased in recent years. For example, PEC are cornerstone components in most renewable energy installations, and they play a vital role in automotive electrification. Both applications have significantly grown over the past years [3]–[5]. Additionally, they are used in industrial electric drives in order to improve efficiency. This is an especially important application, since these types of drives consume most of the electric energy produced world wide.

To date, research in power electronics has focused on the improvement of performance and reliability, the inclusion of new technologies, and the development of novel converter topologies and control strategies. However, not much attention has been given to converter cost [6], apart from studies dealing exclusively with the minimization of the material cost of the active components of the converters (i.e., transistors, diodes, inductors, etc.).

At least two approaches have been taken to accomplish this cost minimization. The first one uses a component database [7]–[10]. In these works, the cost of a specific component is expressed as a function of a limited number of representative parameters, but information about the used databases and the purchasing volumes at which the costs of the components are taken is scarce.

The second approach is to minimize a quantity that is known to be tightly related to the converter's cost. In [11], the total required semiconductor chip area for different converter topologies is compared and used to determine the cost effectiveness of a solution. It is worth noting that the semiconductor devices are one of the main cost-drivers in most converter topologies and that their chip area correlates directly with their cost. This work is further expanded in [6] where comprehensive cost models for power electronics components are presented. Figures for cooling systems and basic components such as bare dies and core materials are included, providing valuable input data to estimate the material cost of the active components in the converter. All the costs are provided for large volumes.

Although the semiconductor components constitute one of the main cost drivers when the converter is produced in large quantities, the investment required for production machines, tooling, fixtures, and test equipment drives the costs significantly at lower production volumes. Regardless of production volumes, the selection of the correct production process to suit the desired output is important in minimizing total converter cost. Moreover, the impact of low power components such as gate drivers, control, sensing, and communication devices is more pronounced in converters with low power rating.

These factors are not considered in the works cited so far. Thus, a complete cost estimation of PEC that includes the effect of production volume, converter layout, and component selection has not been presented yet. The need for this type of cost model is well established in the literature [12].

The work presented in this paper aims to include all the aforementioned aspects into a comprehensive methodology to estimate the cost of a PEC. The presented model is intended to be used within optimization loops to pinpoint sweet spots in a given solution space, as well as in combination with similar calculations for other components in the design of larger systems.

Manuscript received July 15, 2016; revised September 29, 2016; accepted December 19, 2016. Date of publication January 11, 2017; date of current version June 23, 2017. This work was supported by Swedish Energy Agency (Energimyndigheten). Recommended for publication by Associate Editor B. Chen.

G. Domingues-Olavarría, A. Reinap, and M. Alaküla are with the Department of Biomedical Engineering, Division Industrial Electrical Engineering and Automation, Lund University, Lund 22362, Sweden (e-mail: gabriel.domingues@iea.lth.se; avo.reinap@iea.lth.se; mats.alakula@iea.lth.se).

P. Fyhr and M. Andersson are with the Department of Mechanical Engineering, Division of Production and Materials Engineering, Lund University, Lund 22362, Sweden (e-mail: pontus.fyhr@iprod.lth.se; mats.andersson@iprod.lth.se).

Color versions of one or more of the figures in this paper are available online at http://ieeexplore.ieee.org.

Digital Object Identifier 10.1109/TPEL.2017.2651407

For these reasons, expedite execution is a priority and accuracy in the selection or design of components is secondary.

The goal of the model is to quickly and yet accurately estimate the cost of a possible solution in early design stages or in the study of technology transitions rather than to provide an optimized and detailed final design.

II. Methodology

In order to develop a complete understanding on the factors driving the cost of a PEC, an activity-base costing approach is adopted [13].

The first step in the cost estimation procedure is to define the basic characteristics of the converter under study. Knowing the topology of the converter is essential since it provides information on the layout and required set of components. Although several topologies can achieve the same type of energy conversion, their advantages and drawbacks have to be pondered beforehand in order to select the most beneficial topology for the application. Alternatively, an external loop can be added to the cost estimation process to optimize the selection of the topology. However, this work focuses only on estimating the cost of a predefined converter topology. In a similar manner, the operating point(s) and modulation scheme have to be specified in advance, due to the fact that they have great influence on determining the stresses over the different components. Additionally, information about the operating conditions and available cooling needs to be provided in order to ensure that the converter can operate effectively in the targeted environment and that the housing fulfills the demands of the application. Finally, the expected sales volumes are included to account for their impact on the selection of manufacturing processes and their impact on final cost of the converter.

After all the input parameters are defined, the next step consists on determining which components need to be designed and which can be selected directly from a component database. The general approach is that all the signal and control components (i.e., microcontroller, voltage and current sensors, CAN transceiver, etc.) are selected from a component database while power electronics components (i.e., power modules, inductors, transformers, dc-link capacitors, snubbers, filters, etc.) are designed and optimized to work under the operating point and predefined conditions.

Once all the components are either selected or designed, the layout is established based on the size of the components and the topology of the converter. The size of the control PCB is determined as a function of the components that must be mounted and the required connections to other components. At this point, the sizes of all the components are available and their layout is known, so the process continues with the sizing of the housing and cold plate or heat sink dimensions. Finally, the selection of manufacturing and assembly processes required for the producing of magnetic components, PCB, housing, and cooling is optimized for the targeted production volumes.

The final step involves adding the cost of manufacturing, assembly, and quality assurance to the material cost (of components) to obtain the complete manufacturing cost. An overview of the presented methodology is shown in Fig. 1. A detailed explanation of all the processes involved in the presented cost estimation procedure is provided in the upcoming sections.

III. Component Modeling and Sizing

This section describes the sizing methodology for the design of the power electronics components.

A. Semiconductor Devices

This paper focuses on power levels ranging from some tens of kilowatt to a few hundred. In this range, the dominant enclosure for semiconductor devices is the power module. This type of packing provides a good thermal conductivity between the semiconductor device and the heatsink or cold plate, which enables higher power densities. Alternatively, to reduce costs, discrete devices packed in through-hole enclosures can be used in conjunction with PCBs in low power applications. However, the advantages of this implementation are significantly reduced when several devices need to be connected in parallel [14]. For the exposed reasons, and to allow the cost model to be valid in a wide power range, this work assumes power modules to be the package of choice for semiconductor devices.

With the package defined beforehand, the challenge is to determine the minimum size of the semiconductor device that would fulfill the necessary requirements under the specified operating conditions. In order to achieve this, a similar approach as the one presented in [11] is adopted, as illustrated in the left part of Fig. 1.

The size of the semiconductor influences the losses and thermal characteristics of the device. In order to model these effects, a database of components is created and their attributes are correlated with their die area. Interpolation is used to estimate the attributes of devices that are not among the initial set of samples but are within the size range of the semiconductors in the database. Since most datasheets do not specify the area of the semiconductor, a relationship between the nominal current and semiconductor area is extracted from bare die datasheets (see Fig. 2).

The next step consists on modeling the losses as function of the operating conditions and chip area. In line with standard procedure in the literature, only the switching and conduction losses are considered when computing the total power losses in the semiconductor device.

Equation (1) shows how the conduction losses are computed for a semiconductor device. The rms and average current (I_{rms} and I_{ave}) are given by the operating point and modulation scheme while the resistance and voltage are properties that depend on the device size and characteristics. For both IGBTs and diodes, the collector–emitter or forward resistance, respectively, depends on the voltage rating of the device and the chip area, as it can be observed in Fig. 3. On the other hand, the device voltage (forward voltage for diodes and collector–emitter voltage for IGBTs) depends primarily on its voltage rating. Additionally, other factors such as temperature have an effect in these two parameters

$$P_{\text{cond}T/D} = R_{\text{ce}/f} I_{\text{rms}}^2 + V_{\text{ce}/f} I_{\text{ave}}. \tag{1}$$

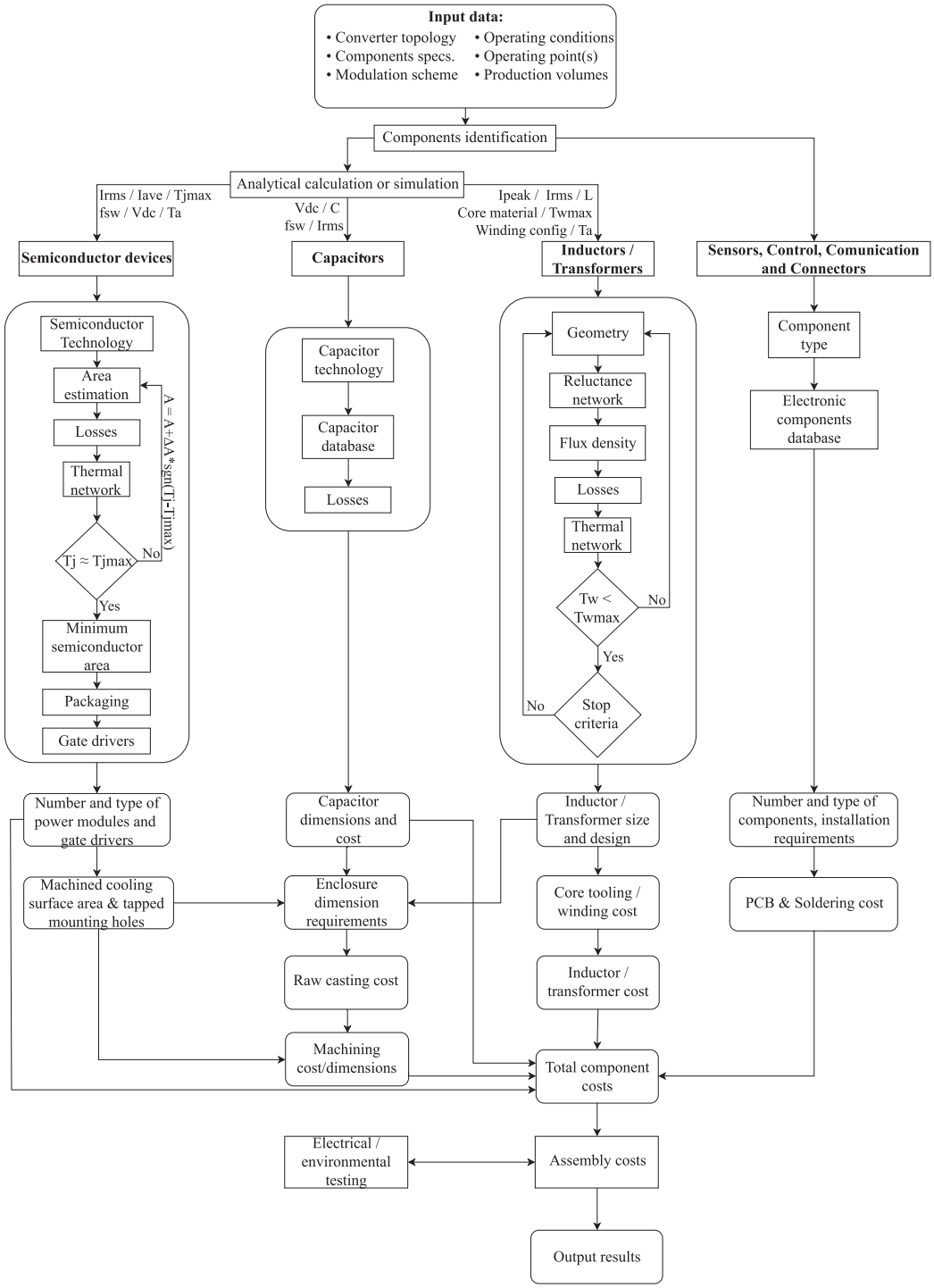

Fig. 1. Flowchart describing the design and manufacturing of the main electrical components of the converter as well as the assembly and testing of the complete converter.

The switching losses are described in (2). The switching frequency f_{sw} is a parameter defined beforehand. T and V represent the operating temperature and blocking voltage while T_{ref} and V_{ref} are the reference values at which the energy losses are defined in the datasheet. k_t and k_v are the temperature and voltage compensation constant [16]. Finally, the energy losses are represented by E_{sw}. This last parameter is described as a function of the current and chip area of the device as it can be seen in Fig. 4 where the losses for diodes and IGBTs rated for 600 and 1200 V are depicted. Note that the data are fitted to the surfaces with a coefficient of determination greater than 0.94 in all cases

$$P_{\text{sw}} = f_{\text{sw}} E_{\text{sw}} \left(\frac{V}{V_{\text{ref}}} \right)^{k_v} (1 + k_t (T - T_{\text{ref}})) \,. \tag{2}$$

It is worth mentioning that the presented energy losses are taken directly from datasheets. Hence, they are measured under

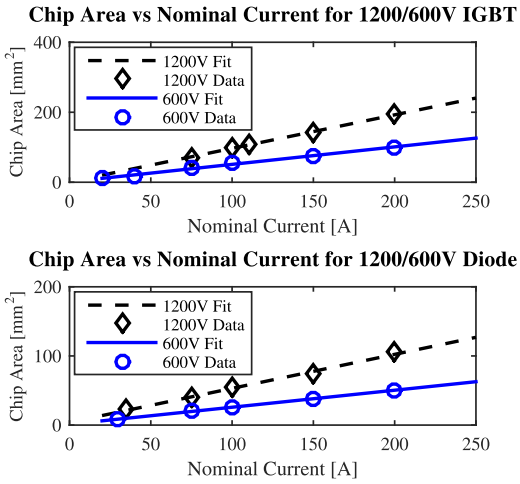

Fig. 2. Area as function of nominal current for 600/1200-V IGBTs and diodes. Data from [15].

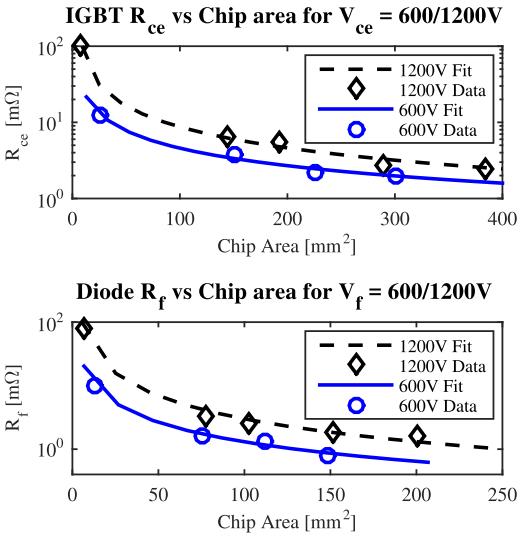

Fig. 3. On-state resistance as function of die area for 600/1200-V IGBTs and diodes. Data from [15].

specific testing conditions and by use of a recommended value for the gate resistor. Terms to compensate for different operating temperatures and voltages are included in (2). However, if it is desired to use a different gate resistor it is necessary to experimentally measure the losses in the devices and add them to the database creating a new surface on top or below the ones presented in Fig. 4. In this paper, the converters are calculated assuming that the recommended gate resistor is selected.

The thermal resistance between the junction of the semiconductor device and the heatsink is mostly determined by the structure of the power module. The silicon itself only accounts for about 4% of the total thermal resistance [16]. Considering this, the thermal resistance between the junction and the heatsink of any semiconductor device is modeled solely as a function of its area, as shown in Fig. 5.

Once the loss and thermal modeling of semiconductor devices is complete, an iterative procedure is carried out in order to determine the minimum size of the semiconductor device required for a given application. The iterative procedure uses as input data the technology of semiconductor, currents, blocking voltage, switching frequency, and heatsink temperature. As the first step of this process, a preliminary estimation of the area is carried out and the losses produced by a chip of that size are estimated. By use of those losses and the heatsink temperature, the junction temperature is calculated (3). If T_j is greater or lower than the predefined maximum value, the size of the chip is adjusted again and the process is repeated until the junction temperature is around the desired level. At this point, the size of the semiconductor device has been optimized for the application. This process can be observed in the semiconductor section of Fig. 1. It is important to keep in mind that this sizing procedure is based on average temperature and losses, meaning that peak temperatures can exceed the maximum allowable junction temperature. This procedure is then repeated for each semiconductor in the converter. It worth noting that the described loss estimation and sizing methodology for IGBTs and diodes is also extendable to other transistor and diode technologies or voltage ratings, as long as it is described how their chip area affects their thermal and electrical characteristics

$$T_j = T_a + R_{\text{th,js}} P_{\text{loss}}. \tag{3}$$

After the total area of all the semiconductor devices is estimated, it is possible to calculate the number and size of power modules required to accommodate all the devices. The ratio between the power module and semiconductor area is usually in the range of 4–10. Reducing this ratio increases the thermal coupling between chips but reduces the size and/or number of power modules which effectively reduces the cost. Finding an optimal value for this ratio requires an in-depth thermal analysis which would be very time consuming. Therefore, a fixed value based on experience is selected in this work. With the size and number of power modules and semiconductor devices calculated, it is possible to estimate the cost of the power module using the cost model presented in [6].

B. Power Capacitor

Among the bulkiest and most expensive components of the PEC are the power capacitors. Together with the magnetic components (i.e., transformers and inductors) they determine, to a great extent, the required dimensions of the housing.

In order to select the most appropriate capacitor for the application, several aspects need to be considered. First, the capacitor technology needs to be defined. The most common type of capacitors used in power electronics are metalized film and electrolytic. The most suited technology varies depending on the application. However, in general it can be said that electrolytic capacitors have a greater capacitance density, shorter life expectancy, and lower current handling capabilities than film capacitors.

The second aspect to consider is the voltage rating of the capacitor. It has to be selected to provide a margin with respect to the nominal operating voltage. This allows the capacitor to cope with voltage transients and extends its life expectancy. Third, the capacitor must withstand the current stresses it is subject

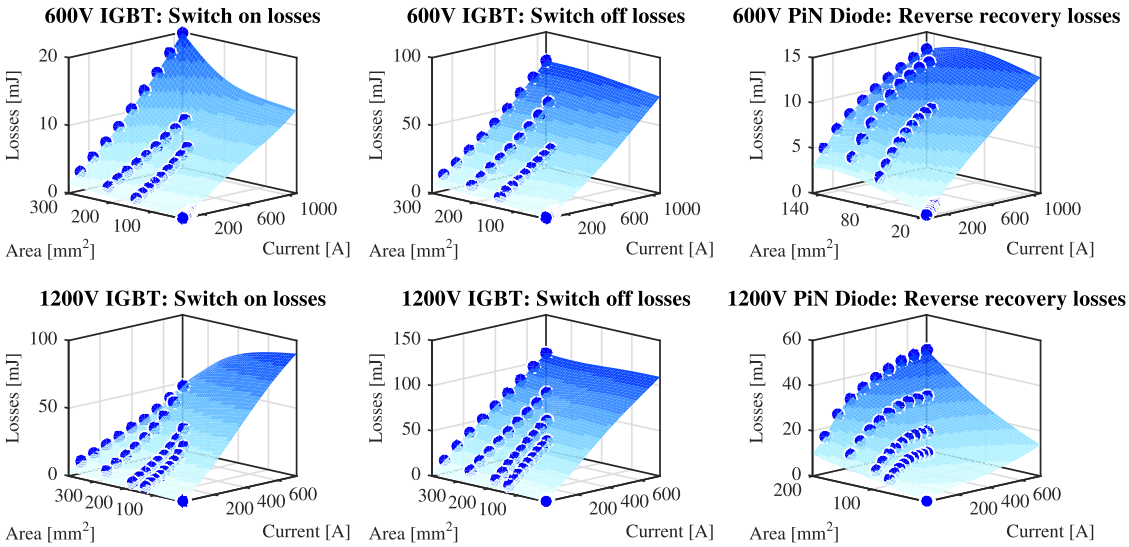

Fig. 4. Switching energy losses for 600-V and 1200-V IGBT's and diodes as function of chip area and current. The blue dots are the losses extracted from the datasheets and the surfaces are the fitted losses. Data from [15].

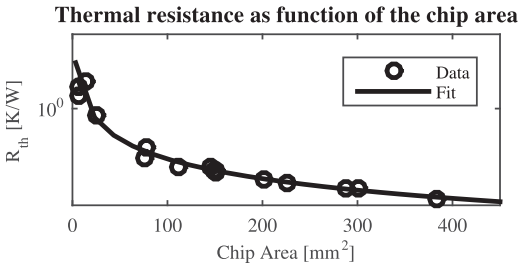

Fig. 5. Thermal resistance between the junction of the semiconductor and the heatsink as function of the chip area. Data from [15].

to without overheating or accelerating its degrading process. As a first approximation, the rated rms current at the operating frequency and temperature can be used as a guide [17], although in a final design a thorough analysis of the losses and the thermal cycling is required. Finally, it needs to be ensured that the peak and inrush currents are within the limits of the selected capacitor.

In order to demonstrate how the capacitor technology influences its characteristics, Fig. 6 presents the volume and current handling capabilities of capacitors for dc-link application as function of technology, voltage, and capacitance. It can be noticed that for a given voltage rating, both the volume and current are quite linear with the capacitance. Deviations from this approximation can be explained by the fact that capacitor manufacturers do not optimize the packaging of each capacitor independently but instead they try to reduce the number of packaging alternatives that they offered in their product range. It is worth mentioning that similar figures can be obtained for capacitors meant to be used in other applications such as snubbers and filters. However, they are not presented in this paper for the sake of brevity.

A database including capacitor technology, volume, cost, voltage rating, and current handling capabilities is created in order to determine the capacitor characteristics for a given application. Interpolation is used to estimate the values if the required capacitor is not among the set of samples used to construct the database. This approach is feasible in reality since most capacitor manufacturers offer the alternative to produce tailored capacitors as long as they utilize existing technologies and the production volumes are large enough. Once all the characteristics of the capacitor are defined, its cost can be estimated by means of the cost model presented in [6].

C. Inductors and Transformers

The procedure to design inductors and transformers is well known and vastly explained in the literature [22]–[24]. As for the previous components, this paper focuses on producing an estimation of the true size with material specifications and winding arrangement for the inductor/transformer rather than on providing a final, complete, and detailed design.

In this context, the employed sizing procedure starts with collecting the required input data. Operating conditions and frequency, available cooling, current waveforms and transformation ratio or inductance are among the essential parameters required to determine the size and eventually the cost of the specific inductor/transformer.

The winding configuration is defined beforehand by the designer, who has to ponder the benefits and drawbacks of one configuration respect to the others in the application under consideration. For example, the main benefit of round wires is their lower cost compared to alternative solutions. On the other hand, Edge and foil winding provide a high fill factor, while at the same time relieving some of the current penetration issues at high frequencies that may increase the losses in round conductors. Finally, litz wires are an interesting alternative to further reduce the ac losses in the winding at the expense of a higher cost and lower fill factor. If the designer wishes to optimize the winding selection, an external loop can be added to the design of the magnetic component in order to test different winding configurations.

By intention, the core size is not discretized by standard sizes according to the manufacturers' databases. Therefore, it is

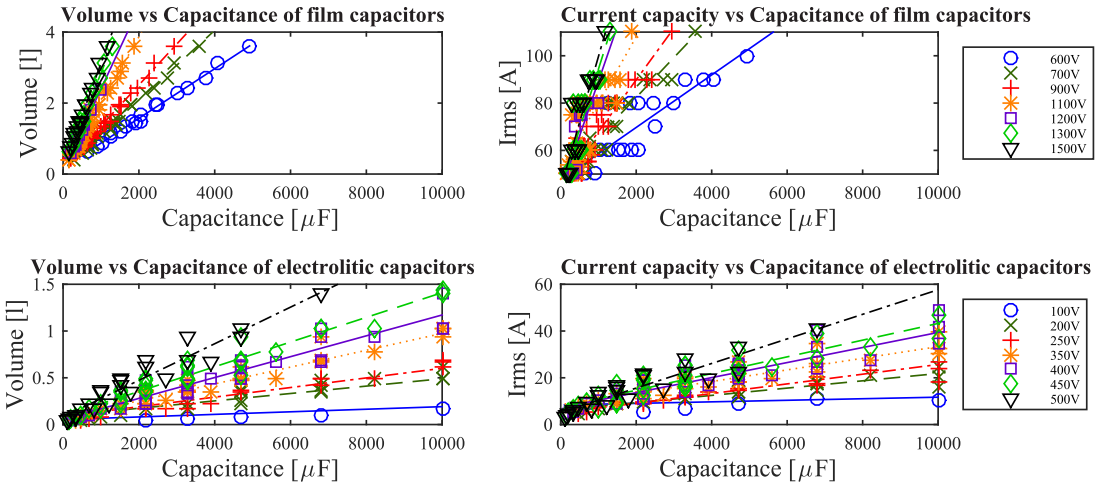

Fig. 6. DC-link capacitors characteristics [18]–[21].

assumed that the core dimensions can be freely varied. The core consists of either pressed and sintered iron powder of different kinds, or stacked electrical steel sheets of various thicknesses and grades. Reluctance networks are used to calculate the air gap(s) length (if applicable), the operating flux densities, and to define possible winding arrangements that allow us to achieve the desired inductance/transformation ratio.

Thermal networks are used to ensure that the temperature in the hot spot of the proposed inductor/transformer is below the maximum allowable limits. To accurately calculate the copper losses, the 2-D analytic approach presented in [25]–[27] is taken, which allows us to include the effect of fringing flux from the air gap, proximity, and skin effect. On the other hand, the core losses are calculated using the modified Steinmetz equation (MSE) [28].

The use of thermal and reluctance networks is preferred over finite element analysis due to fast execution and sufficiently high accuracy. However, it is worth noting that additional steps need to be performed prior to the production of a final design. For example, the stray inductance and capacitance need to be calculated, the estimated losses can be compared with results from finite element simulations (see Fig. 7 where the analytic outcome of loss estimation is compared to FEA), the manufacturability of the proposed winding solution needs to be verified, etc.

The size of these components is determined as follows: first, a large set of core geometries is proposed. Each one of the proposed cores in then evaluated to see if it fulfils the requirements of the application; the number of turns, airgap length (if applicable), and operating flux densities are calculated. Once this is done, the copper and core losses are calculated and it is verified that the hot spot temperature is below the maximum allowable temperature for the selected winding class. From the initial set of proposed core geometries, a subset of feasible cores is found. The final step is to select one geometry from this subset of feasible cores according to a criterion predefined by the designer. This criterion can be highest efficiency, lowest weight, or minimum cost.

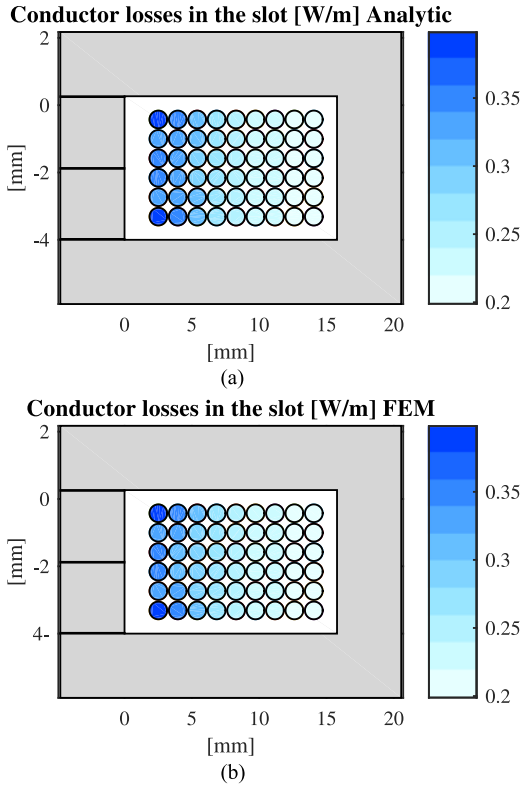

Fig. 7. Comparison between the copper losses calculated analytically and by use of FEM. Each conductor carries a triangular wave current with a duty cycle of 25%, an average value of 3.3 A, a peak of 4 A, and a frequency of 10 kHz. The maximum discrepancy in the calculations occurs close to the airgap where the analytic method overestimates the losses up to 10% with respect to the losses obtained by FEM. The average error in the winding is below 4.5%. (a) Analytic calculation of the copper losses in each conductor. (b) FEM calculation of the copper losses in each conductor.

D. Housing

Depending on the level of protection required by the application [29], two different types of housings are included in this work: cast and folded sheet metal. The first type is preferred in applications where the converter needs to be completely isolated

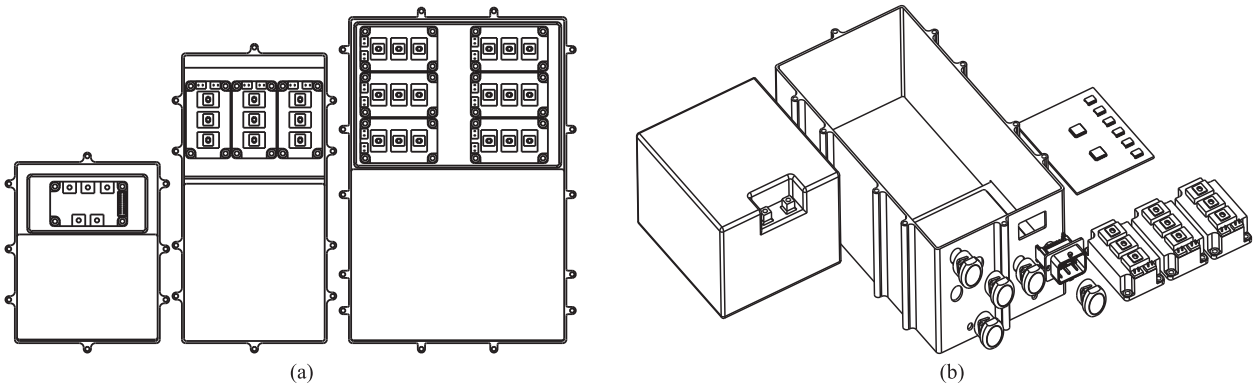

Fig. 8. Generic housings and enclosures arrangements. (a) Enclosure layouts for a two-level inverter at various power levels. (b) A generic cast housing together with power modules, dc-link capacitor and control PCB.

from the environment it is operating in (e.g., electric vehicle, outdoor PV, etc.). The second type of housing offers a lower cost but can only be used in applications with lower isolation requirements (e.g., indoors industrial installation, home appliances, etc.).

For air cooled converters, an extruded aluminum heatsink is used. The area of the heatsink is determined by the area of the bottom plate of the housing. The height is set so that the thermal resistance of the heatsink combined with the calculated losses yield to the desired heatsink temperature [30]. The airflow is assumed to be constant at all sizes and the cost of the fan is not included in the estimation. On the other hand, for liquid cooled converters the cooling channels are cast under the main housing and a lid with a rubber seal is used to avoid coolant leakage. The cost of the pump and heat exchanger are not included in the estimation.

The size of either type of housing is mainly governed by the size of the capacitors, amount of power modules, and magnetic components (inductors, transformers). The design is scalable in length, width, and height in order to accommodate components, as well as increasing the surface area for cooling, see Section IV-C and Fig. 8(a), (b). For example, a converter layout, similar to those shown in Fig. 8(a), is chosen from a list of predefined layouts, depending on the number and size of power modules and magnetic components required by the converter. This layout, including thermal expansion padding and internal clearance for connectors, determines the part of the enclosure length as well as the width available for the capacitor bank. The height of the capacitor bank is set to a fixed value in order to provide space above the power modules for the bus-bars and control PCB. The capacitor bank length is then scaled to the requirements described in Section III-B. A fixed wall thickness as well as mounting points and lids are added to give the final converter dimensions.

E. Control Unit

The control unit consists of a PCB, populated with gate drivers, one or several microcontrollers (if redundancy is needed), a communication controller (Ethernet for industrial applications, CAN for automotive), connectors as well as a number of discrete components (e.g., capacitors, diodes, resistances, etc.) needed by the drivers and controllers. The placement of the components in the PCB is dictated by a set of predefined rules. For the case presented in Section VI, the number of gate drivers and connectors required by the amount of power modules, as determined in Section III-A, gives the control board width, the level of redundancy, connectors, controllers, and padding for routing and power dissipation give the length.

TABLE I
COST MODEL PARAMETERS

Parameter	Unit	Description
k_i	€	Unit cost
K_A	€	Annuity cost of tool investment
K_B	€	Working material cost
K_{CP}	€	Running costs during production
K_{CS}	€	Running costs during downtime
K_D	€	Wage costs
n_{pA}	–	n batches until maintenance
t_0	min	Cycle time
N_0	units	Production volume
q_s	–	Standstill factor
q_Q	–	Rejection rate

IV. MANUFACTURING

As the cost-model described in this work handles converters of different topologies as well as voltage and current levels, a scalable generic layout is chosen in order to include the variations in the materials used, processing time, and assembly. The sizing of the power components governs these processes in a multitude of ways, as illustrated in Fig. 1. A representation of how the power module layout and dc-link capacitor size affects the converter enclosure, for a two-level inverter is shown in Fig. 8(a).

Each of the processes involved in the production of the converter is modeled using (4) [31], [32], the parameters of which are listed in Table I. Each of these inputs are specific to the

TABLE II
PROCESS INPUT DATA FOR INCLUDED PROCESSES

	Investment cost (€)	Cycle time (s)	Personnel (n)	Yield (%)
Sand cast	1500–2000	60–300	2-3	92–96
Die cast	10 000–50 000	20–120	1–2	98–99
Machining	30 000-50 000	120–1800	1	99
PCB mfg.	2000–4000	90–180	1–2	99
PCB solder	8000–15000	30–120	1–2	98–99
Bus bar	6000–12000	90–240	1	98
Electrical asm.	20 000–35 000	180–420	1	95–98
Final QA	30 000-100 000	45–225	1	98
Spool winding	150 000-300 000	60–250	1	98
Edge winding	100 000-200 000	180–420	1	98
Foil winding	100 000-200 000	100–300	1	98

current production-process denoted by i. When a sequence of processes are performed, the value added is included as cost of material K_B in the subsequent process, see (5). Input data for various processes are listed in Table II. All investments are considered to be annuitized over 5 years

$$k_i(N_0) = \frac{K_A}{N_0}\left[\frac{1}{n_{pA}}\right] + K_B\left[\frac{1}{1-q_{Qi}}\right] + K_{CP}\left[\frac{t_{0i}}{1-q_{Qi}}\right] + K_{CS}\left[\frac{t_{0i}q_{si}}{(1-q_{Qi})(1-q_{si})}\right] + K_D\left[\frac{t_{0i}q_{si}}{(1-q_{Qi})(1-q_{si})}\right] \quad (4)$$

$$K_{Bi}(N_0) = k_{i-1}(N_0). \quad (5)$$

A. PCB

The bare PCBs are printed with solder paste, SMD component population is performed with pick and place, finally reflow soldering completes the boards. The gate and sensor connections to the power-modules are manually assembled ribbon cables to connectors on the control board.

B. Power Connection

The power components are connected via shaped (edge bending, sheet forming, and stamping) copper bus bars. Its dimensions are sized to match the requirements placed by the physical layout of the power-modules, connectors, and capacitor, power module termination size and current requirements for the given power-output.

C. Casting

The casting must encapsulate the converter components, providing both environmental sealing, electromagnetic-interference (EMI) shielding and cooling of primarily the power-modules and the dc-link capacitor, as well as inductors/transformers where applicable. In this work, an aluminum casing with a water-jacket cooled fin structure is used, this can be produced using a combination of casting and machining.

The casting methods included in this work are sand casting and die casting. Die casting requires less machining in order to achieve the desired surface tolerances for sealing and power module cooling. Both processes assume access to a foundry, and the investment made is only considering the tooling specific to the parts produced for the converter.

The lid is assumed to use the same part for both the top and bottom part of the casing, thus doubling the output of the lid tool.

Many previous works have implemented the selection of appropriate casting processes for geometries of varying size, complexity, and production volumes [33].

It is worth noting that the cycle-times of both casting processes vary with the size and surface area of the casting to be produced, see Table II. This in turn is governed by the layout of the power components, as shown in Fig. 8(b). The generated generic layouts could be further optimized to increase power density. However, such optimization should be performed in final the design of a specific converter.

D. Machining

The machining requirements on the cast parts that are used in the casing consist of face milling surfaces that require tighter tolerances than the as-cast state. In the production cost calculations in this work, these are defined as the surfaces where the power modules are mounted for both sand and die-cast parts, as well as the sealing surfaces for the lids in the sand cast parts. In addition to face milling, drilling and tapping operations are needed for parts that are mounted with screws, such as the power modules, lids, inductors, and capacitors. End milling of ports for power and signal connectors and water jacket fittings is also required.

Machining cycle times t_0 are based on a cutting speed of 2000 m/min for milling with a feed of 2000 mm/min [34]. Drilling is performed with a cutting speed of 150 m/min and a feed of 0.16 mm/rev [35].

Die cast parts are assumed to be machined in one setup, using face milling in two passes to achieve sufficient tolerances for heat transfer from the power modules with normal thermal interface materials. Sand cast parts are machined in two setups, as the sealing surfaces against the lids also need to be machined.

E. Metal Folding

An unfolded metal sheet is cut by a flexible process, such as laser cutting, which can reach speeds of up to 10 m/min. At very high production volumes, this may be replaced with a fixed tooling process, such as blanking. After cutting, the sheet is folded in an edge-press, deburred at critical locations and coated.

F. Magnetic Components

Winding of the magnetic components can be performed by spool winding, edge winding, or foil winding. When spool

winding is employed, the desired amount of parallel strands, of the desired thickness, are wound onto an injection moulded bobbin. The connectors are crimped after winding. The cycle times depend on the selected winding. Round conductors present lower cycle times which further reduces the cost of this winding configuration (approx. 0.5s/turn). Edge, foil, and litz winding usually present higher cycle times (approx. 5 s/turn for edge winding and litz wire, 2 s/turn for foil winding), see Table II.

The flux conducting core material of the magnetic components consists of either stamped and bonded electric steel sheet, or powder-based sintered cores. For steel sheets, the relatively simple geometry allows inexpensive cutting tools, though the tool costs increases with the surface area of the cut geometry. Sintered materials are limited in size by the volume of the sintered material and the press available in preparation of the green body. After assembly of the cores and windings, all magnetic components are potted.

G. Quality Assurance

After assembly, each converter is subjected to one to three quality assurance inspections, the first one for the electrical circuits and control, which is applicable to all converters. The second one is only applicable where water cooling is employed, and consists on a cooling circuit leak test. The third inspection applies to converters which are classified as sealed to some degree (i.e., IP 6X), where the ingress protection from splashed water and/or submersion protection is tested.

V. Model Limitations and Assumptions

A. Assumptions

In order to simplify the process of estimating the cost of a PEC, several assumptions are necessary:

1) the gate resistance used for driving the transistors is the same as the one used for providing the losses in the datasheets;
2) the semiconductors devices are sized so their average operating temperature is below a maximum limit;
3) custom power modules can be purchased and set up costs are included;
4) capacitors can be selected from a continuous range of capacitance/voltage values;
5) the geometry of a powder core can be selected arbitrarily;
6) the manufacturing is carried out in Europe;
7) the cost of workshop space is not accounted for;
8) the cost of bulk materials is fixed;
9) shipping and handling costs are not included.

B. Purchased Parts

A number of components included in the model are considered to be purchased from external suppliers, as their design is not specific for the application and they are produced at large scale. These include:

1) capacitors, resistors and diodes;
2) fully assembled PCB(s);
3) extruded aluminum heatsinks;
4) gate drivers and sensors;
5) microcontrollers and transcievers
6) connectors;
7) custom made power modules.

C. Processes Carried Out In-House

A list of the processes assumed to be done in-house is:

1) machine or fold the components of the housing;
2) stamp the laminations and wind the coils for the magnetic components;
3) potting the capacitor bank, inductors, and transformers;
4) bus-bar shaping;
5) assembly;
6) electrical and environmental sealing testing.

D. Overheads and Profits

Overhead costs and profit margins depend to a great extent on the specific characteristics of the company that manufactures the equipment and the type of deal they reach with the customer. For these reasons, the presented cost estimation focuses only on determining the manufacturing cost.

VI. Example of Application and Discussion

In this section, the presented cost model is used to estimate the cost of a PEC for a hybrid or full electric vehicle. This application represents an interesting case of study since it is highly sensitive to cost variations and some cost projections are available. For example, in [36] is reported that by 2015 a reasonable figure for an automotive PEC is 8 $/kW.

The selected converter topology is a three-phase two-level voltage source converter and the modulation scheme is SV-PWM. The converter is assumed to be liquid cooled with a cold plate temperature of 80 °C. Due to the harsh environment that the converter is expected to operate in, an IP67 ingress protection level is selected.

For the sake of brevity, the sensitivity analysis is only carried out based on production volumes, rated power, and dc-link voltage level. The switching frequency remains the same for all converters at 10 kHz and the semiconductor devices are Si Diode and field stop IGBT4. Film self-healing capacitors are used in the dc-link.

Fig. 9 shows the estimated manufacturing cost of PEC rated for different powers and voltages under varying yearly production volumes. The first thing that can be noticed is that, for high voltage converters, the rated voltage has an impact in the cost. This can be explained by looking into the way that the two main components of the converter interact to the changes in the voltage/current combinations. Semiconductor devices normally lose current handling capabilities and increase their cost for the same die area at higher voltages, but simultaneously, as the voltage increases the current demands in the converter are reduced due to the fact that the power is maintained constant.

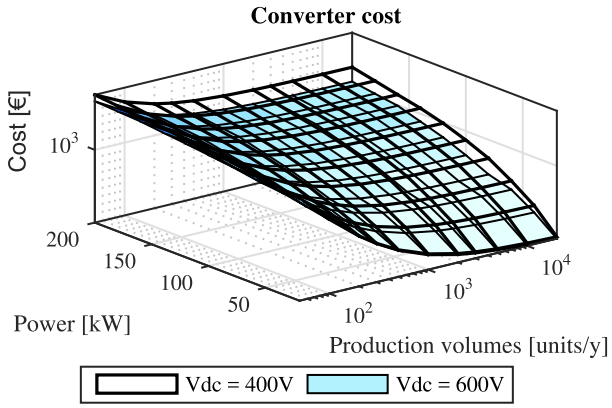

Fig. 9. Manufacturing cost of three-phase automotive converter for EV/HEV application.

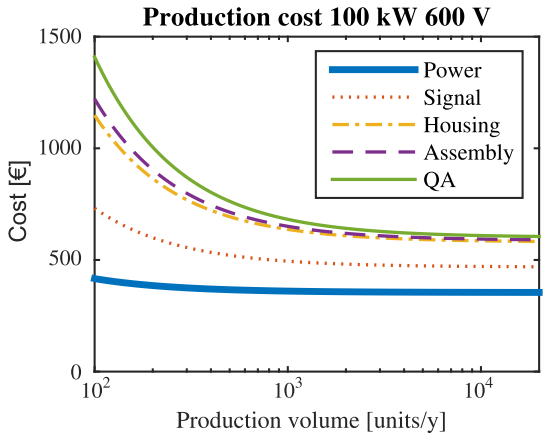

Fig. 11. Resulting cost breakdown over production volume. For a two-level 100-kW 600-V automotive inverter.

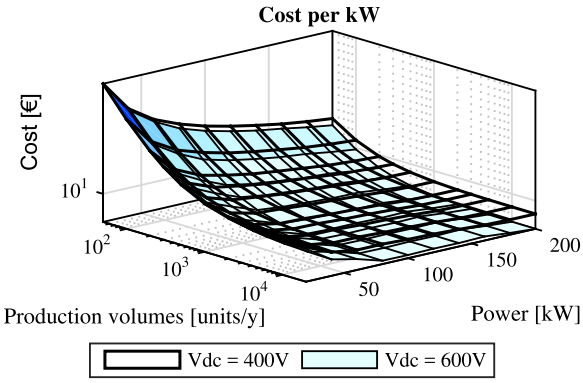

Fig. 10. Manufacturing cost per kW of three-phase automotive inverter for EV/HEV application.

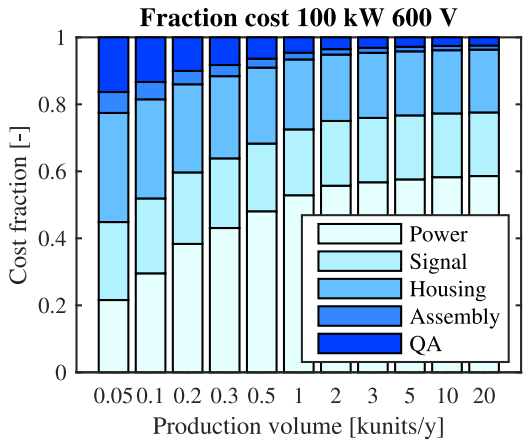

Fig. 12. Cost fractions of total over production volumes. For a two-level 100-kW 600-V automotive inverter.

This yields to a slight increase in the cost of semiconductors for converters of lower voltages. On the other hand, the capacitor volume and current handling capabilities increase together with the voltage ratings but the capacitance requirement drops due to a drop in the current through the dc-link capacitor, reducing the final cost of the dc-link capacitor for converters of higher voltages.

The second aspect that is important to observe in Fig. 9 is that, at low production volumes, the impact of the rated power in the cost is low. The reason for this phenomenon is that at low production volumes, most of the cost of the converter is related to covering the investments in production machines, tooling, fixtures, and test equipment and the cost of the converters components only represents a small fraction of the total cost. However, with an increase in the production volumes, the investment costs are distributed among a larger number of units and the cost of an individual converter drops significantly. This drop on the production cost also increases the cost difference between converters of different power levels.

A commonly used figure of merit for automotive PEC is their cost per kilowatt. Fig. 10 presents the cost per kilowatt for the same converters presented in Fig. 9 under the same voltage, power, and production volumes scenarios. It can be noticed that the cost per kilowatt drops together with increased rated power of the converter. the main reason for this behavior is that some of the converter's costs do not scale with power (i.e., control unit, transceivers, sensors) meaning that they have a greater impact in the total cost of lower power converters. Therefore, the use of constant figures of cost per kW, as it is usually done in the literature, can yield to misleading results. For this reason, the use of more accurate cost models, like the one presented in this work, is encouraged. Alternatively, if high level of detail in the cost estimation is not required, a linear cost function with a term that does not depend on the power can provide a better approximation than figures of cost per kilowatt.

A breakdown of costs incurred in each production step for the 100-kW converter is shown in Euro in Fig. 11 and in relative cost in Fig. 12. Both figures show that the power components (switching, capacitor and bus-bars) make up less than one-third of the costs at low production volumes, but

over two-thirds at a higher production output. This is due to the high investment levels required for tooling, production, and qualification equipment, which is distributed over each unit produced, with some refurbishment and service of the equipment over its lifetime. On the other hand, the purchased parts, such as power-modules, capacitors, connectors, etc., do not have the same scaling relationship with production volume. The signal & components cost lumps the finished control PCB, including transceivers, gate drivers, internal and external connectors.

Housing includes the finished milled casting and lid, with correct mating surfaces for power modules and tapped holes for screw mounts. Assembly contains the additional costs for assembling the parts into the housing, completing the circuits, and mounting connectors.

Quality control contains one to three steps depending on the type of housing, circuit testing, and case sealing, both for the water jacket and ingress protection, where applicable.

VII. Conclusion

A methodology for a complete cost estimation of PEC is presented and the sizing, selection, and manufacture of the different components are explained. This model provides a complete view of all the aspects affecting the cost of the converter from design decisions to selection of manufacturing process and expected production volumes. The aforementioned aspects make the presented work a useful tool that allows the designer to evaluate the cost effectiveness of different converter designs in various production systems, given an estimate of sales volume.

Due to the modular nature of the proposed framework, it is possible to modify the sizing procedures in order to include a higher level of detail if computational times are not critical or if the number of converters that are being studied is reduced. This flexibility allows the designer to perform both a preliminary screening over a wide range of possible solutions and a detailed optimization of a selected design.

The modular nature also allows the selection of manufacturing processes and automation levels to suit the desired production volumes of both individual components and finished converters, as well as the possibility to compare designs suited for different environments.

The presented model is used to estimate the cost of inverters for automotive applications. It is shown how some important factors such as power, production volumes, rated voltage, etc. affect the final cost of the converter. Additionally, it is worth noting that the predicted cost per kW is similar to figures available in the literature at high power and large production volumes and that it differs significantly in the opposite case. Therefore, when performing optimization of a full electric or hybrid vehicle, reported figures of $€/kW$ must be handled with care and adjustments to account for power and expected production volumes must be made. For this reason, the use of more accurate cost models, like the one presented in this work, is encouraged.

Appendix

The data presented in Figs. 9 and 10 are summarized in Tables III and IV.

TABLE III
Cost of a 600-V Three-Phase Two-Level Voltage Source Converter for EV/HEV Application

Power-Units	100	1000	5000	10 000	20 000
20 kW	1023	296	232	224	220
40 kW	1120	393	328	320	316
60 kW	1228	501	436	428	424
80 kW	1290	563	498	490	486
100 kW	1409	682	617	609	605
120 kW	1537	810	745	737	733
140 kW	1655	928	863	855	851
160 kW	1790	1063	998	990	986
180 kW	1862	1135	1071	1063	1059
200 kW	1939	1212	1148	1140	1136

TABLE IV
Cost of a 400-V Three-Phase Two-Level Voltage Source Converter for EV/HEV Application

Power-Units	100	1000	5000	10 000	20 000
20 kW	1032	305	240	232	228
40 kW	1169	442	378	369	365
60 kW	1313	586	521	513	509
80 kW	1483	756	691	683	679
100 kW	1633	906	841	833	829
120 kW	1787	1060	996	988	984
140 kW	1926	1199	1135	1127	1123
160 kW	2046	1319	1255	1247	1243
180 kW	2186	1459	1394	1386	1382
200 kW	2337	1610	1545	1537	1533

References

[1] United Nation Framework for Climate Change (UNFCC), "Adoption of the paris agreement." Paris, France, 2015. [Online]. Available: http://unfccc.int/resource/docs/2015/cop21/eng/l09r01.pdf

[2] C. Miller, "3.02–energy resources and policy: Vulnerability of energy resources and resource availability—Fossil fuels (oil, coal, natural gas, oil shale)," *Climate Vulnerability*, 2013, pp. 37–51. [Online]. Available: http://www.sciencedirect.com/science/article/pii/B978012384703400304X

[3] Global Wind Energy Council (GWEC), "Global wind statistics 2014," Brussels, Belgium, 2015. [Online]. Available: http://www.gwec.net/wp-content/uploads/2015/02/GWEC_GlobalWindStats2014_FINAL_10.2.2015.pdf, Accessed on: Jan. 2016.

[4] Solar Power Europe, "Global market outlook for solar power/2015-2019," Brussels, Belgium, 2015. [Online]. Available: http://helapco.gr/pdf/Global_Market_Outlook_2015_-2019_lr_v23.pdf, Accessed on: Jun. 2016.

[5] A. T. de Almeida, F. J. T. E. Ferreira, and A. Q. Duarte, "Technical and economical considerations on super high-efficiency three-phase motors," *IEEE Trans. Ind. Appl.*, vol. 50, no. 2, pp. 1274–1285, Mar. 2014.

[6] R. Burkart and J. Kolar, "Component cost models for multi-objective optimizations of switched-mode power converters," in *Proc. Energy Convers. Congr. Expo.*, Sep. 2013, pp. 2139–2146.

[7] S. Busquets-monge *et al.*, "Power converter design optimization," *IEEE Ind. Appl. Mag.*, vol. 10, no. 1, pp. 32–38, Jan. 2004.

[8] S. Busquets-Monge *et al.*, "Design optimization of a boost power factor correction converter using genetic algorithms," in *Proc. 17th Annu. IEEE Appl. Power Electron. Conf. Expo.*, 2002, vol. 2, pp. 1177–1182.

[9] S. Busquets-Monge *et al.*, "Design of a boost power factor correction converter using optimization techniques," *IEEE Trans. Power Electron.*, vol. 19, no. 6, pp. 1388–1396, Nov. 2004.

[10] A. Kulkarni and A. Bazzi, "A building-block approach to efficiency and cost models of power electronic systems," in *Proc. 29th Annu. IEEE Appl. Power Electron. Conf. Expo.*, Mar. 2014, pp. 2727–2734.
[11] T. Friedli and J. Kolar, "A semiconductor area based assessment of ac motor drive converter topologies," in *Proc. 24th Annu. IEEE Appl. Power Electron. Conf. Expo.*, Feb. 2009, pp. 336–342.
[12] J. W. Kolar, J. Biela, S. Waffler, T. Friedli, and U. Badstuebner, "Performance trends and limitations of power electronic systems," in *Proc. 6th Int. Conf. Integrated Power Electron. Syst.*, Mar. 2010, pp. 1–20.
[13] A. Niazi, J. S. Dai, S. Balabani, and L. Seneviratne, "Product cost estimation: Technique classification and methodology review," *J. Manuf. Sci. Eng.*, vol. 128, no. 2, pp. 563–575, 2006.
[14] D. O. Neacsu, *Switching Power Converters: Medium and High Power*. Boca Raton, FL, USA: CRC Press, 2013.
[15] "Infineon IGBT datasheets," [Online]. Available: http://www.infineon.com, Accessed on: Jan. 2016.
[16] A. Wintrich, U. Nicolai, W. Tursky, and T. Reimann, "Application manual power semiconductors," ISLE, 2011.
[17] Electronicon, "Capacitors for power electronics application notes selection guide," Gera, Germany, 2013, [Online]. Available: http://www.electronicon.com/fileadmin/inhalte/pdfs/downloadbereich/Katalog/neue_Kataloge_2011/application_notes.pdf, Accessed on: Dec. 2015.
[18] "Metallized polypropylene (pp)—capacitors in cylindrical case," [Online]. Available: http://www.wima.com/EN/WIMA_DC_Link_MKP_6.pdf, Accessed on: Jan. 2016.
[19] "Screw terminal aluminum electrolytic capacitors," [Online]. Available: http://www.kemet.com/Lists/ProductCatalog/Attachments/389/KEM_A4031_ALS 30_31.pdf, Accessed on: Jan. 2016.
[20] "Screw terminal aluminum electrolytic capacitors," [Online]. Available: https://en.tdk.eu/inf/20/30/db/aec_2013/B44020_B44030.pdf, Accessed on: Jan. 2016.
[21] "Film capacitors," [Online]. Available: https://en.tdk.eu/inf/20/50/ds/B2562_.pdf, Accessed on: Jan. 2016.
[22] N. Mohan and T. M. Undeland, *Power Electronics: Converters, Applications, and Design*. New York, NY, USA: Wiley, 2007.
[23] C. W. T. McLyman, *Transformer and Inductor Design Handbook*. Boca Raton, FL, USA: CRC Press, 2011.
[24] E. L. Barrios, A. Urtasun, A. Ursua, L. Marroyo, and P. Sanchis, "Optimal dc gapped inductor design including high-frequency effects," in *Proc. 41st Annu. Conf. IEEE Ind. Electron. Soc.*, Nov. 2015, pp. 003 928–003 933.
[25] J. Mhlethaler, J. W. Kolar, and A. Ecklebe, "Loss modeling of inductive components employed in power electronic systems," in *Proc. 2011 IEEE 8th Int. Conf. Power Electron. Conf.*, May 2011, pp. 945–952.
[26] J. Hu and C. R. Sullivan, "Optimization of shapes for round-wire high-frequency gapped-inductor windings," in *Proc. 33rd IAS Annu. Meeting Ind. Appl. Conf.*, Oct. 1998, vol. 2, pp. 907–912.
[27] W. Chen, X. Huang, and J. Zheng, "Improved winding loss theoretical calculation of magnetic component with air-gap," in *Proc. 7th Int. Power Electron. Motion Control Conf.*, Jun. 2012, vol. 1, pp. 471–475.
[28] J. Reinert, A. Brockmeyer, and R. De Doncker, "Calculation of losses in ferro- and ferrimagnetic materials based on the modified steinmetz equation," *IEEE Trans. Ind. Appl.*, vol. 37, no. 4, pp. 1055–1061, Jul. 2001.
[29] *Degrees of Protection Provided by Enclosures*, Indian Standard 60529,1989.
[30] U. Drofenik, G. Laimer, and J. W. Kolar, "Theoretical converter power density limits for forced convection cooling," in *Proc. Int. Conf. Power Electron., Intell. Motion, Power Quality*, 2005, pp. 608–619.
[31] J.-E. Ståhl *et al.*, *Metal Cutting Theories and Models*. Fagersta, Sweden: Division of Production and Materials Engineering and Seco Tools, 2012.
[32] M. Jönsson, "Cost-conscious manufacturing models and methods for analyzing present and future performance from a cost perspective," Ph.D. dissertation, Lund University, Lund, Sweden, 2012. [Online]. Available: https://lup.lub.lu.se/search/publication/030ee6a6-0edb-490c-afbd-2fe7f6 81e330
[33] S. Darwish and A. El-Tamimi, "The selection of the casting process using an expert system," *Comput. Ind.*, vol. 30, no. 2, pp. 77–86, 1996.
[34] H. Kishawy, M. Dumitrescu, E.-G. Ng, and M. Elbestawi, "Effect of coolant strategy on tool performance, chip morphology and surface quality during high-speed machining of {A356} aluminum alloy," *Int. J. Mach. Tools Manuf.*, vol. 45, no. 2, pp. 219–227, 2005.
[35] M. Nouari, G. List, F. Girot, and D. Coupard, "Experimental analysis and optimisation of tool wear in dry machining of aluminium alloys," *Wear*, vol. 255, no. 712, pp. 1359–1368, 2003.
[36] C. L. Whaling, "Technology roadmap analysis 2013: Assessing automotive technology R&D relevant to doe power electronics cost targets," Status Report Presentation, 2013.

Gabriel Domingues-Olavarría was born in Venezuela in 1989. He received the M.Sc. (*summa cum laude*) degree in electronic engineering from Simón Bolívar's University, Miranda, Venezuela, in 2013. He is currently working toward the Ph.D. degree in the Division of Industrial Electrical Engineering and Automation, Faculty of Engineering, Lund University, Lund, Sweden.

Pontus Fyhr was born in 1984 in Sweden. He received the M.Sc. degree in mechanical engineering from Lund University, Lund, Sweden, in 2009. He is currently working toward the Ph.D. degree at the Division of Production and Materials Engineering, Faculty of Engineering, Lund University.

Avo Reinap was born in Estonia in 1973. He received the Diploma degree in engineering and the M.Sc. degree in power engineering from Tallinn University of Technology, Tallinn, Estonia, in 1998 and 2000, respectively. He received the Ph.D. degree in technology from Lund University, Lund, Sweden, in 2005.

From 2005 to 2010, he was an Associate Professor in the Department of Electrical drives and Power Electronics, Tallinn University of Technology and from 2007 to 2011 a Postdoctoral Fellow in the Division of Industrial Electrical Engineering and Automation, Faculty of Engineering, Lund University.

Mats Andersson was born in 1961 in Sweden. He received the Graduate degree in mechanical engineering from Lund University, Lund, Sweden, in 1988 and the Ph.D. degree in metal cutting in 1993.

He is currently an Associate Professor in the Division of Production and Materials Engineering. He has specialized in process dynamics in machining operations and measuring of high-frequency cutting forces. His current research focuses on development manufacturing technologies for electric drives and on development of soft magnetic composites.

Mats Alaküla was born in 1961 in Sweden. He received the Graduate degree in electrical engineering from Chalmers University of Technology in Gothenburg, Gothenburg, Sweden, in 1986. He received the Licentiate degree from Chalmers University of Technology in 1989 and the Ph.D. degree from Lund University, Lund, Sweden, in 1993.

Since 1994, he has been a Full Professor in the Division of Industrial Electrical Engineering, Faculty of Engineering, Lund University. He is the Coordinator for the Electrical Machines and Drives area in the Swedish Hybrid Vehicles Center. At present time, he combines his academic duties with a position as a Senior Specialist in Hybrid Technology at Volvo Powertrains.